
Clinical Translation of an Albumin-Binding PET Radiotracer ^{68}Ga -NEB

Jingjing Zhang^{1,2}, Lixin Lang², Zhaohui Zhu¹, Fang Li¹, Gang Niu², and Xiaoyuan Chen²

¹Department of Nuclear Medicine, Peking Union Medical College Hospital (PUMCH), Chinese Academy of Medical Sciences and Peking Union Medical College (CAMS and PUMC), Beijing, China; and ²Laboratory of Molecular Imaging and Nanomedicine, National Institute of Biomedical Imaging and Bioengineering, National Institutes of Health, Bethesda, Maryland

Suitably labeled Evans blue dye has been successfully applied to evaluate cardiac function, vascular permeability, and lymphatic imaging in preclinical settings. This study documented the first-in-human application of ^{68}Ga -1,4,7-triazacyclononane-*N,N,N'*-triacetic acid (NOTA)-NEB. **Methods:** The NOTA-conjugated truncated form of Evans blue, NEB, was labeled with ^{68}Ga and tested in BALB/C mice for dynamic PET and ex vivo biodistribution studies. Three healthy volunteers (2 men and 1 woman) underwent 90-min whole-body dynamic PET. The absorbed doses for major organs and whole body were calculated using OLINDA/EXM software. Eleven patients with focal hepatic lesions diagnosed by enhanced CT or MR imaging were subjected to whole-body PET/CT acquisitions at 30 min after intravenous injection of 111–148 MBq (3–4 mCi) of ^{68}Ga -NEB. **Results:** NEB dye was labeled with ^{68}Ga (half-time, 68 min) with high yield and purity. After intravenous injection, ^{68}Ga -NEB formed a complex with serum albumin, thus most of the radioactivity was retained in blood circulation. The tracer was demonstrated to be safe in both healthy volunteers and recruited patients without side effects or allergies. Among the 11 patients, hemangiomas showed much higher ^{68}Ga -NEB signal intensity than the surrounding normal hepatic tissues, whereas no apparent difference between lesions and hepatic tissues was identified on ^{18}F -FDG PET. All other focal hepatic lesions including hepatocellular carcinoma, hepatic cysts, and neuroendocrine tumor liver metastases showed negative ^{68}Ga -NEB contrast to hepatic tissues. **Conclusion:** As a blood-pool imaging agent, ^{68}Ga -NEB is safe to use in the clinic, and our preliminary studies demonstrate the value of differentiating hepatic hemangioma from other benign or malignant focal hepatic lesions. Easy labeling with different positron emitters of various half-lives, excellent pharmacokinetics, and imaging quality warrant further clinical applications of NEB-based PET tracers.

Key Words: truncated Evans blue; albumin; blood pool; first-in-human; hemangioma

J Nucl Med 2015; 56:1609–1614

DOI: 10.2967/jnumed.115.159640

Angiography plays a critical role in screening, diagnosis, treatment planning, and prognosis in vascular diseases. With blood-pool contrast agents, CT and MR imaging angiography provide excellent spatial and temporal resolution of arteries and veins, thus replacing the invasive conventional angiography (1). However, the relatively low sensitivity of CT and MR imaging requires administration of large quantities of contrast agents, which increases the risks of allergic reaction or nephrotoxicity (2).

Radionuclide angiography, with $^{99\text{m}}\text{Tc}$ -labeled red blood cells (RBCs) as the dominant imaging agent, has been used clinically as early as 1958 for determining total blood and plasma volumes, cardiac output, protein turnover studies, heart and great vessel delineation, and localization of cerebral neoplasms (3). Compared with SPECT, PET is more sensitive and has higher spatial resolution with clinical scanners.

A few PET blood-pool imaging tracers have been introduced for labeling RBCs. For example, carbon monoxide containing either ^{11}C or ^{15}O has been used to label RBCs for PET (4). However, because of their short half-lives (20.4 min for ^{11}C and 2.05 min for ^{15}O), these tracers can be used only in centers with an in-house cyclotron. Furthermore, the need for administration of the gaseous form of carbon monoxide by inhalation necessitates sophisticated equipment for human as well as animal studies (5). The use of RBCs for blood-pool imaging also presents significant risks to both the patient receiving the product and the operator handling radiolabeled RBCs. Thus, there is a critical need for a clinically practicable PET blood-pool imaging agent for angiography.

Instead of RBCs, serum albumin has been labeled with various positron-emitting radionuclides for PET (6–10). The general strategy was to conjugate albumin with radioisotopes in vitro and then inject the labeled albumin intravenously for imaging. However, the unfavorable pharmacokinetics of these albumin-based tracers, such as high liver accumulation, suggests that the albumin structure may have been partially disrupted during the bioconjugation and labeling process. Moreover, in vitro protein labeling is time consuming and requires multiple steps of purification and quality control.

Alternatively, we have developed a method for in vivo labeling of the endogenous albumin by conjugating a cyclic chelator, 1,4,7-triazacyclononane-*N,N,N'*-triacetic acid (NOTA), on the truncated form of Evans blue (EB), denoted as NEB (11). EB dye has high affinity for serum albumin and has been used clinically to determine blood volume (12,13). Although recently discontinued in clinical practice, EB is still used as a sensitive marker of protein leakage from the vascular lumen in a variety of tissues during inflammation and traumatic injury (14,15). The radiolabeling

Received Apr. 20, 2015; revision accepted Jul. 17, 2015.

For correspondence or reprints contact either of the following:

Fang Li, Peking Union Medical College, 9 Dongdan 3rd Alley, Dongcheng, Beijing, China.

E-mail: lifang@pumch.cn

Xiaoyuan Chen, National Institutes of Health (NIH), 35A Convent Dr., GD937, Bethesda, MD 20892-3759.

E-mail: shawn.chen@nih.gov

Published online Aug. 6, 2015.

COPYRIGHT © 2015 by the Society of Nuclear Medicine and Molecular Imaging, Inc.

of ^{18}F was achieved by the formation of ^{18}F -aluminum fluoride complex (16–18). The entire labeling process takes about 20–30 min without the need of high-performance liquid chromatography purification (11). After intravenous injection, ^{18}F -AIF-NEB complexed with serum albumin quickly, and thus most of the radioactivity remained in the blood circulation. ^{18}F -AIF-NEB has been successfully applied to evaluate cardiac function in a myocardial infarction model and vascular permeability in inflammatory and tumor models (11). In a more recent study, we applied ^{18}F -AIF-NEB along with the EB dye for lymphatic imaging after local injection (19). In view of the great success of NEB in preclinical investigations, we moved forward to clinical applications. Instead of ^{18}F , we used ^{68}Ga as the positron emitter, because with ^{68}Ga the cyclotron was nonessential and because of the feasibility of kit formulation (20).

MATERIALS AND METHODS

Preparation of ^{68}Ga -NEB

NEB was synthesized according to a method described in our previous publication (11). ^{68}Ga was eluted from a $^{68}\text{Ge}/^{68}\text{Ga}$ generator (ITG) using 0.05 M HCl and mixed with 1.25 M NaOAc buffer to adjust the pH value to 4.0. The mixture was then directly transferred to a 1-mL plastic tube containing 30 μg of NEB. After shaking, the mixture was incubated in a heating block at 100°C for 10 min. Then the reaction mixture was cooled down, dissolved in sterile phosphate-buffered saline, and passed through a 0.22- μm aseptic filtration membrane. The quality control was performed with analytic high-performance liquid chromatography and thin-layer chromatography (Bioscan, USA). $\text{CH}_3\text{OH}:\text{NH}_4\text{OAc}$ (v/v 1:1) was used as the developing solution for thin-layer chromatography. The radiochemical purity was greater than 95%.

Preclinical PET Imaging

All animal studies were conducted in accordance with the principles and procedures outlined in the *Guide for the Care and Use of Laboratory Animals* (21) and were approved by the Institutional Animal Care and Use Committee of the Clinical Center, National Institutes of Health. For dynamic PET scans, 4 BALB/C mice were injected intravenously with 1.85 MBq (50 μCi) of ^{68}Ga -NEB under isoflurane anesthesia. A 60-min list-mode acquisition was performed with an Inveon PET scanner (Siemens Preclinical Solutions). Images were reconstructed using the 2-dimensional ordered-subsets expectation maximum algorithm without attenuation or scatter correction. Regions of interest (ROIs) over major organs were drawn on decay-corrected whole-body coronal images for each PET scan, using vendor software (ASI Pro 5.2.4.0; Preclinical Solutions, Siemens). The radioactivity concentration (accumulation) within a tumor or an organ was obtained from mean pixel values within the multiple-ROI volume, after conversion of the values to MBq/mL/min using a conversion factor. The conversion to MBq/g/min assumed a tissue density of 1 g/mL. Imaging ROI-derived percentage injected dose per gram was calculated by dividing the ROIs by the administered activity (22).

Volunteers and Patient Recruiting

This first-in-human study was approved by the Institutional Review Board of Peking Union Medical College Hospital, Chinese Academy of Medical Sciences, and Peking Union Medical College. All subjects signed a written informed consent form and were informed of the benefits and possible risks of participating in the study. Three healthy volunteers (2 men and 1 woman) were enrolled to validate the safety of ^{68}Ga -NEB. No fasting, hydration, or other specific preparation was requested on the day of imaging. For all 3 healthy volunteers, the blood pressure, pulse, respiratory rate, and temperature were measured before and after injection of tracer ^{68}Ga -NEB. In addition, liver function,

kidney function, routine blood, and urine tests were performed in 2 of the 3 volunteers before and 24 h after the scans. Any unusual or adverse clinical symptoms volunteers complained about or physical signs including the blood pressure, pulse, respiratory rate, temperature, liver function, kidney function, routine blood tests, and urine tests were included and recorded in the clinical evaluation. Any unusual or adverse clinical symptoms were recorded on the day of imaging and during the 2-wk follow-up period.

Eleven patients with hepatic space-occupying lesions were recruited. The inclusion criteria included the following: being identified with hepatic lesions by MR imaging or CT (the lesions were suspected as hemangioma, or hepatic malignancy, and needed differentiation from other benign diseases with surgery or biopsy); at least 18 y old; and able to provide basic information and sign the written informed consent form. The final diagnosis was based on pathologic results of surgical removal or biopsy. Among the recruited patients, 4 patients were diagnosed with hemangioma, 5 with primary hepatic carcinoma, 1 with neuroendocrine tumor liver metastases, and 1 with hepatic cyst. All the recruited patients underwent surgery after the PET scans, as recommended by their clinicians.

PET Imaging Procedures

All 3 healthy volunteers underwent whole-body PET acquisitions (Biograph mCT PET/CT system; Siemens) at multiple time points after tracer injection. After the whole-body low-dose CT scan (140 kV; 35 mA; pitch, 1:1; layer, 5 mm; layer spacing, 3 mm; matrix, 512 \times 512; field of view, 70 cm), 111–148 MBq (3–4 mCi) of ^{68}Ga -NEB were injected intravenously. The whole body (from the top of the skull to the middle of the femur) of each volunteer was covered by 7 bed positions. The acquisition duration was 40 s/bed position for the 5-, 10-, and 15-min time points and 2 min/bed position for the 30-, 45-, 60-, 75-, and 90-min time points.

All patients with hepatic lesions underwent whole-body PET/CT acquisitions at 30 min after intravenous injection of 111–148 MBq (3–4 mCi) of ^{68}Ga -NEB, with each bed position lasting for 2 min. The acquisition field covered from the top of the skull to the middle of the femur with 6 or 7 bed positions, depending on the height of the patient. An ^{18}F -FDG PET/CT image was acquired with the same patients within 1 wk.

Image and Data Analysis

A Siemens MMWP workstation was used for postprocessing. Visual analysis was used to determine the general biodistribution and the temporal and intersubject stability. The volume of interest of normal organs/tissues and concerned lesions was drawn on the serial images. The radioactivity concentration and standardized uptake value (SUV) in the volumes of interest were obtained through the software. All quantitative data were expressed as mean \pm SD.

The dosimetry calculation was performed according to the European Association of Nuclear Medicine dosimetry guidance (23). The decay-uncorrected time-activity curve was generated on the basis of the SUV of each organ. The SUVs were converted to MBq/MBq based on organ weight from the adult male phantom (73.7 kg of body weight) and the adult female phantom (56.9 kg of body weight) provided by OLINDA/EXM (version 1.1; Vanderbilt University) (24,25). The time-integrated activity coefficient (residence time) of each organ was determined by fitting the data using a biphasic exponential model provided by the software. The urine bladder volume was determined by reconstructed PET/CT images, and the residence time was calculated by the trapezoidal method using GraphPad Prism (version 4.0; GraphPad Software, Inc.). The void time was set as 60 min. The remainder of body was calculated for each time point as the decayed value of the original injected activity minus activity present in the identified source organs. Then the absorbed doses were calculated by entering the

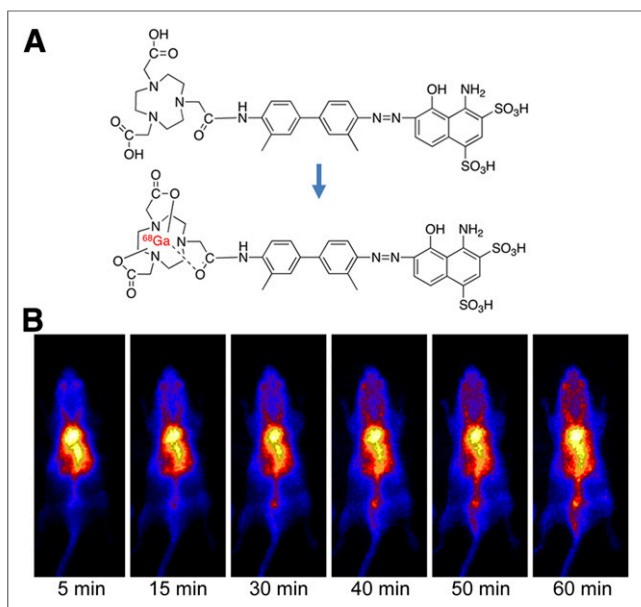


FIGURE 1. (A) Chemical structure of NEB and radiolabeling of NEB with ^{68}Ga . (B) Representative coronal maximum-intensity-projection images of 60-min dynamic ^{68}Ga -NEB PET of normal BALB/C mouse.

time-integrated activity coefficient for all source organs into OLINDA/EXM for either a 73.7-kg adult male or 56.9-kg adult female.

RESULTS

Chemistry and Radiochemistry

The structure and radiolabeling of NEB with ^{68}Ga are presented in Figure 1A. The whole labeling process of ^{68}Ga -NEB took about 30 min, with a radiochemical purity of greater than 95% as determined by both analytic radio-high-performance liquid chromatography and radio-thin-layer chromatography. ^{68}Ga -NEB showed good stability in mouse serum after 120 min of incubation (Supplemental Fig. 1; supplemental materials are available at <http://jnm.snmjournals.org>).

In Vivo Dynamic PET Imaging and Biodistribution in Normal Mice

To investigate the pharmacokinetics of ^{68}Ga -NEB, we performed 1-h dynamic PET in healthy BALB/C mice. After tail vein injection, most of the radioactivity from ^{68}Ga -NEB was retained in the blood circulation, including the ventricles of the heart, major arteries, and blood-enriched organs, during the entire period of observation (Fig. 1B; Supplemental Fig. 2).

To estimate the safe dose for clinical use, we performed an ex vivo biodistribution study in normal BALB/C mice. The absorbed doses for major organs and whole body were then extrapolated to an adult human male of a body weight of 73.7 kg using OLINDA/EXM software. The mean dose range from 5 mice at each time point is listed in Supplemental Table 1. The kidneys received the highest absorbed doses (mean absorbed dose, 0.104–0.135 mSv/MBq), resulting from abundant blood supply and tracer excretion through the renal urinary tract. The mean effective dose of ^{68}Ga -NEB was 0.0151–0.0159 mSv/MBq. With an injected dose of 185 MBq (5 mCi), the patient would be exposed to an effective radiation dose of 2.94 mSv, which is much lower than the dose limit of 20 mSv for the second risk category

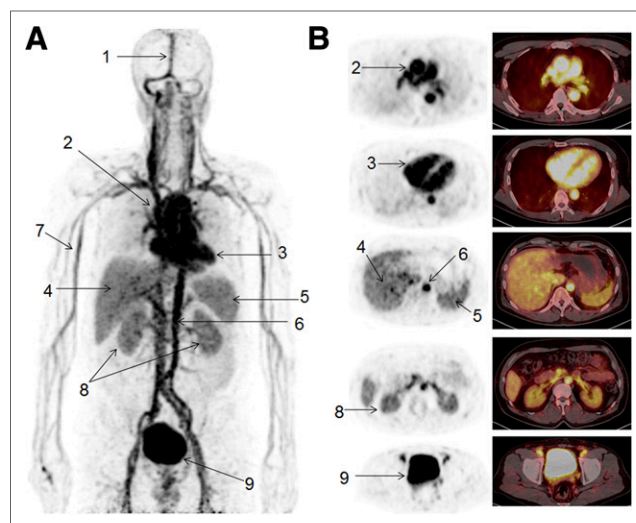


FIGURE 2. (A) Coronal maximum-intensity-projection image of male volunteer at 30 min after intravenous administration of 138.75 MBq (3.75 mCi) of ^{68}Ga -NEB. Principal organs and regions of uptake are labeled: superior sagittal sinus (1), arch of aorta (2), cardiac ventricles (3), liver (4), spleen (5), abdominal aorta (6), limb vessels (7), kidneys (8), and bladder (9). (B) Corresponding axial PET and PET/CT fusion images at key levels to reflect arch of aorta, cardiac ventricles, liver and spleen, kidneys, and bladder.

defined by the 2007 International Commission on Radiological Protection (26).

Healthy Volunteers and Dosimetry

With a mean injected dose of 139.5 ± 10.36 MBq (3.77 ± 0.28 mCi), no adverse symptoms were noticed or reported during the entire procedure and 2-wk follow-up, demonstrating the safety of the tracer. A representative 2-dimensional projection PET image acquired at 30 min after intravenous administration of ^{68}Ga -NEB is presented in Figure 2. Cardiac ventricles, major arteries, and

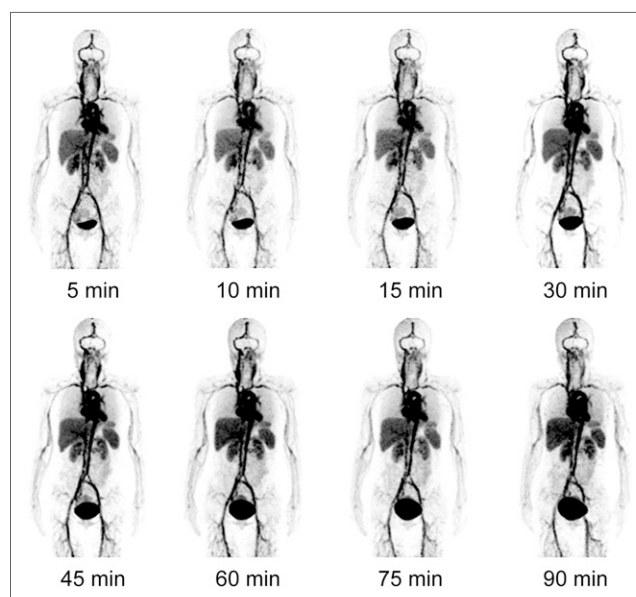


FIGURE 3. Multiple-time-point whole-body maximum-intensity-projection PET images of female healthy volunteer at 5, 10, 15, 30, 45, 60, 75, and 90 min after intravenous administration of ^{68}Ga -NEB.

TABLE 1
Biodistribution of ⁶⁸Ga-NEB in Healthy Volunteers (SUV, *n* = 3)

Time (min)	Blood	Lung	Liver	Spleen	Kidneys	Stomach	Intestinal	Pancreas	Bone	Muscle
5	7.97 ± 0.15	1.53 ± 0.15	3.80 ± 0.44	4.10 ± 0.36	4.40 ± 0.26	1.23 ± 0.15	1.73 ± 0.25	2.13 ± 0.40	2.10 ± 0.26	0.53 ± 0.21
10	7.53 ± 0.25	1.47 ± 0.29	3.70 ± 0.61	4.07 ± 0.47	4.23 ± 0.49	1.50 ± 0.20	1.57 ± 0.12	2.03 ± 0.15	1.93 ± 0.12	0.60 ± 0.10
15	7.17 ± 0.35	1.40 ± 0.17	3.73 ± 0.59	4.00 ± 0.52	4.03 ± 0.50	1.23 ± 0.12	1.73 ± 0.12	1.90 ± 0.26	1.83 ± 0.15	0.60 ± 0.17
30	6.93 ± 0.21	1.30 ± 0.17	3.57 ± 0.46	3.90 ± 0.61	3.77 ± 0.29	1.23 ± 0.06	1.63 ± 0.15	1.67 ± 0.15	1.67 ± 0.15	0.57 ± 0.12
45	6.70 ± 0.26	1.30 ± 0.20	3.50 ± 0.52	3.77 ± 0.57	3.87 ± 0.32	1.23 ± 0.06	1.63 ± 0.06	1.67 ± 0.15	1.50 ± 0.20	0.53 ± 0.06
60	6.20 ± 0.17	1.23 ± 0.06	3.47 ± 0.47	3.73 ± 0.42	3.60 ± 0.10	1.10 ± 0.00	1.47 ± 0.15	1.43 ± 0.15	1.37 ± 0.06	0.50 ± 0.00
75	6.03 ± 0.12	1.10 ± 0.17	3.43 ± 0.49	4.93 ± 2.10	3.43 ± 0.15	1.07 ± 0.12	1.33 ± 0.21	1.37 ± 0.21	1.27 ± 0.12	0.47 ± 0.06
90	5.97 ± 0.15	1.07 ± 0.12	3.33 ± 0.58	3.57 ± 0.55	3.30 ± 0.20	1.03 ± 0.15	1.17 ± 0.32	1.37 ± 0.31	1.23 ± 0.15	0.77 ± 0.64

veins showed the highest signal density. Vessel branches in and out of major organs and limbs can also be clearly identified. The liver, spleen, and kidneys are also visible, with relatively low activity, whereas the bladder showed high activity.

From 5 to 90 min, no dramatic distribution change was observed, confirming the in vivo stability and long blood-pool retention of ⁶⁸Ga-NEB (Fig. 3). Increased bladder accumulation was observed over time. The average SUVs in the major organs and tissues are listed in Table 1. Although the blood vessels in the brain showed high radioactivity, the normal brain tissue had negligible accumulation of ⁶⁸Ga-NEB, indicating that the tracer does not cross the blood–brain barrier.

The mean absorbed radiation doses based on multiple-time-point PET images of 3 volunteers were similar to those based on mouse biodistribution data (Table 2). The major organs that received relatively high doses were the kidneys, liver, spleen, and heart wall. The bladder wall also received high exposure due to renal excretion of the radioactivity (0.0683 ± 0.0090 mSv/MBq). The whole-body absorbed dose was 0.0151 ± 0.0001 mSv/MBq, with an effective dose of 0.0179 ± 0.0003 mSv/MBq.

Differential Diagnosis of Focal Hepatic Lesions

The widespread use of imaging studies has led to an increase in detection of incidental focal hepatic lesions. Differential diagnosis of malignant and benign solid and cystic liver lesions is important for patient management (27). Among the 11 patients with focal hepatic lesions diagnosed by enhanced CT or MR imaging, 4 were with hemangioma. All hemangiomas showed much higher ⁶⁸Ga-NEB signal intensity than the surrounding normal hepatic tissues, whereas no apparent difference between lesions and hepatic tissues was identified on ¹⁸F-FDG PET. The lesions were not discernable on regular CT but showed signal enhancement with CT contrast agent (Supplemental Fig. 3). Hepatocellular carcinoma (HCC) showed high tracer uptake on ¹⁸F-FDG PET but with big variance from patient to patient. ⁶⁸Ga-NEB showed consistently lower HCC uptake than normal hepatic tissue (Fig. 4; Supplemental Fig. 4). Similarly, hepatic cysts and neuroendocrine liver metastases also showed a low lesion-to-background ratio with ⁶⁸Ga-NEB PET (Fig. 4).

Because of the abundant blood supply, normal liver tissue showed prominent ⁶⁸Ga-NEB accumulation with an SUV of 3.73 ± 0.47 (Table 3). The SUV of ⁶⁸Ga-NEB in hemangiomas (6.83 ± 1.38) was much higher than that in the surrounding hepatic tissue (*P* < 0.01). All other focal hepatic lesions including HCC, hepatic cysts, and neuroendocrine tumor liver metastases showed negative contrast to hepatic tissues with SUVs of 2.12 ± 0.16, 2.13, and 2.69 ± 0.44, respectively.

DISCUSSION

This first-in-human study was based on a successful in vivo albumin-labeling strategy with an EB derivative, which formed a complex with serum albumin after intravenous injection (11).

TABLE 2

Absorbed Radiation Doses Per Unit Administered Activity from Intravenous Administration of ⁶⁸Ga-NEB (mGy/MBq, *n* = 3)

Target organ	Mean	SD
Adrenals	0.01393	0.00021
Brain	0.01083	0.00072
Breasts	0.01053	0.00055
Gallbladder wall	0.01530	0.00000
Lower large intestine wall	0.01303	0.00057
Small intestine	0.02523	0.00119
Stomach wall	0.01630	0.00026
Upper large intestine wall	0.01367	0.00042
Heart wall	0.03917	0.00045
Kidneys	0.04617	0.00254
Liver	0.04797	0.00697
Lungs	0.01813	0.00153
Muscle	0.00985	0.00074
Ovaries	0.01337	0.00051
Pancreas	0.02393	0.00255
Red marrow	0.01016	0.00041
Osteogenic cells	0.01590	0.00087
Skin	0.00961	0.00050
Spleen	0.04830	0.00548
Testes	0.01113	0.00055
Thymus	0.01213	0.00055
Thyroid	0.01113	0.00055
Urinary bladder wall	0.06830	0.00904
Uterus	0.01417	0.00055
Total body	0.01507	0.00006
Effective dose equivalent	0.02413	0.00071
Effective dose	0.01786	0.00029

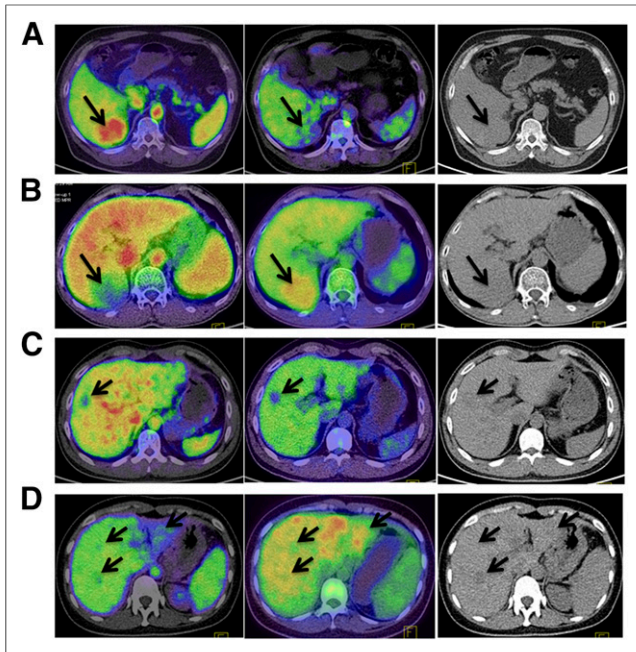


FIGURE 4. Differential diagnosis of focal hepatic lesions using ^{18}F -FDG and ^{68}Ga -NEB PET/CT. (A) Images of hepatic hemangioma: ^{68}Ga -NEB PET/CT (left) shows strong local accumulation of radioactivity with hepatic nodule, whereas ^{18}F -FDG PET/CT (middle) shows relatively low local uptake. Nodule is also identified by CT (right) without much signal contrast. (B) Images of hepatic carcinoma. Lesion shows negative contrast compared with surrounding normal hepatic tissue on ^{68}Ga -NEB PET/CT (left) whereas increased ^{18}F -FDG uptake is observed with ^{18}F -FDG PET/CT (middle). (C) Neuroendocrine tumor liver metastasis. Multiple liver nodules are detected on CT scan (right). ^{68}Ga -NEB PET/CT (left) shows low uptake in all hepatic nodules, compared with mild to moderate uptake in ^{18}F -FDG PET/CT (middle). (D) Hepatic cysts show low uptake of ^{68}Ga -NEB and ^{18}F -FDG.

The labeling was efficient without compromising the physiologic behavior of the protein, thus the emitted radioactive signal reflected accurately the *in vivo* behavior of albumin (11,28). The method also avoided unnecessary cross-contamination from blood products as is the case with labeling of RBCs for blood-pool imaging. For imaging purposes, only a trace amount of the compound was administered so the possible toxicity of the vital dye and potential pulmonary embolism after intravenous injection was completely avoided (29).

Indeed, all healthy volunteers and patients reported no discomfort or adverse clinical events, no elicited acute toxicity, and no allergies. Dosimetry study confirmed the safety with acceptable absorbed doses by critical organs even with multiple injections for 1 patient. With an injected dose of 121–148 MBq (3–4 mCi), a patient would be exposed to a radiation dose of 2.65 mSv, which is much lower than the dose limit as set by the Food and Drug Administration (25).

After intravenous injection, most of the radioactivity was retained in blood circulation because of the stable complexation of ^{68}Ga -NEB with serum albumin. Within a few minutes after tracer injection, the radioactivity reached equilibrium as reflected by the constant high SUV in the blood. A slow but steady clearance of the radioactivity from the blood was observed, which was mainly caused by the turnover of albumin from blood circulation to the interstitial space and slight dissociation of ^{68}Ga -NEB from albumin. Still, the heart-to-liver

ratios at different time points were close to those of *in vitro*-labeled RBCs and significantly higher than those of *in vivo*-labeled RBCs (30), confirming the role of ^{68}Ga -NEB as a blood-pool PET imaging agent.

There are several major applications for a blood-pool imaging agent including evaluation of the cardiac function, detection of vascular anomalies, and localization of neoplasms. Hepatic hemangioma is a vascular anomaly, characterized by multiple vascular channels with a single layer of benign endothelial cells. Consequently, a high level of local accumulation of ^{68}Ga -NEB was observed, making tumors highly visible against the surrounding normal hepatic tissues. Meanwhile, lesions of HCC, hepatic cyst, and hepatic metastases of neuroendocrine tumors showed negative contrast because of the relatively low accumulation of ^{68}Ga -NEB. Although promising, whether the small number of cases will support the claim that ^{68}Ga -NEB PET would be more specific than CT, MR imaging, and ^{18}F -FDG PET in differentiating hemangioma from other focal hepatic lesions remains to be elucidated by future trials with more patients.

The identification of liver lesions is of critical importance because of the increasing incidence of primary hepatic malignancies worldwide and an increase in detection of benign liver lesions by the widespread use of abdomen cross-sectional imaging modalities (31). Although many typical lesions can be detected by traditional imaging tests such as ultrasound, CT, and MR imaging, there remains a challenge to diagnose atypical lesions. For example, hypervascular neuroendocrine tumors often share the same appearance as hemangiomas on MR imaging (32–34). Some atypical hepatic cysts may also show features overlapping with hepatic metastasis from ovarian malignancies (35). The accurate diagnosis of hemangioma with ^{68}Ga -NEB PET can avoid unnecessary overtreatment and biopsy, which has the risk of hemorrhage. In combination with ^{18}F -FDG PET, ^{68}Ga -NEB PET/CT can be of great value for the differential diagnosis of cysts, hemangioma, and other benign hepatic lesions from malignancy, especially in patients with a history of malignancy. It is also predictable that ^{68}Ga -NEB PET will be helpful in diagnosing hemangioma occurring in other organs.

Although only differential diagnosis of hepatic space-occupying lesions was covered by this pilot clinical study, it is natural to foresee the application of ^{68}Ga -NEB PET in the evaluation of cardiac function as a blood-pool imaging agent. Although ^{68}Ga -NEB may not be essential in the detection and staging of malignant tumors, ^{68}Ga -NEB PET will give important information of blood supply and vascular density within the lesions. Moreover, different from RBCs, albumin will extravasate in the presence of leaky blood vessel, which is the basis to use EB to evaluate vascular permeability (36). Thus, ^{68}Ga -NEB PET provides another opportunity to evaluate

TABLE 3
SUVs of ^{18}Ga -NEB and ^{18}F -FDG in Focal Hepatic Lesions (Mean \pm SD)

Hepatic lesions	^{18}Ga -NEB	^{18}F -FDG
HCC ($n = 7$)	2.12 \pm 0.16	5.96 \pm 2.90
Neuroendocrine tumor metastasis ($n = 4$)	2.69 \pm 0.44	2.85 \pm 0.70
Hemangioma ($n = 5$)	6.83 \pm 1.38	1.19 \pm 0.19
Cyst ($n = 1$)	2.13	1.21
Normal hepatic tissue ($n = 11$)	3.69 \pm 0.53	1.80 \pm 0.41

tumor angiogenesis and response to antiangiogenic treatment (37). Another reasonable application is to provide a preoperational and intraoperational guide by mapping sentinel lymph nodes by PET and radioactive detector or optical imaging (27).

CONCLUSION

After successful development of in vivo labeling of albumin with the truncated EB, this is the first report to our knowledge of the clinical applications of ⁶⁸Ga-NEB PET. The tracer was demonstrated to be safe in both healthy volunteers and patients without acute toxicity. This small-scale clinical study substantiates the potential of NEB as a blood volume imaging agent in differentiating hepatic hemangioma from other benign or malignant focal hepatic lesions. Easy labeling with different positron emitters, excellent pharmacokinetics, and imaging quality pave a broad way of clinical applications of NEB-derived PET tracers for blood-pool, vascular permeability, and lymphatic imaging.

DISCLOSURE

The costs of publication of this article were defrayed in part by the payment of page charges. Therefore, and solely to indicate this fact, this article is hereby marked “advertisement” in accordance with 18 USC section 1734. This work was supported by the Intramural Research Program (IRP) of the National Institute of Biomedical Imaging and Bioengineering (NIBIB), National Institutes of Health (NIH). No other potential conflict of interest relevant to this article was reported.

REFERENCES

1. Rubin GD, Leipsic J, Joseph Schoepf U, Fleischmann D, Napel S. CT angiography after 20 years: a transformation in cardiovascular disease characterization continues to advance. *Radiology*. 2014;271:633–652.
2. Hasebroock KM, Serkova NJ. Toxicity of MRI and CT contrast agents. *Expert Opin Drug Metab Toxicol*. 2009;5:403–416.
3. Subramanian KM. Cardiac blood-pool tracers. *J Nucl Med*. 1991;32:480–482.
4. Kearfott KJ. Absorbed dose estimates for positron emission tomography (PET): C¹⁵O, ¹¹CO, and CO¹⁵O. *J Nucl Med*. 1982;23:1031–1037.
5. Herance JR, Gispert JD, Abad S, et al. Erythrocytes labeled with [¹⁸F]SFB as an alternative to radioactive CO for quantification of blood volume with PET. *Contrast Media Mol Imaging*. 2013;8:375–381.
6. Hoffend J, Mier W, Schuhmacher J, et al. Gallium-68-DOTA-albumin as a PET blood-pool marker: experimental evaluation *in vivo*. *Nucl Med Biol*. 2005;32:287–292.
7. Todica A, Brunner S, Boning G, et al. [⁶⁸Ga]-albumin-PET in the monitoring of left ventricular function in murine models of ischemic and dilated cardiomyopathy: comparison with cardiac MRI. *Mol Imaging Biol*. 2013;15:441–449.
8. Okazawa H, Yonekura Y, Fujibayashi Y, et al. Measurement of regional cerebral plasma pool and hematocrit with copper-62-labeled HSA-DTS. *J Nucl Med*. 1996;37:1080–1085.
9. Anderson CJ, Rocque PA, Weinheimer CJ, Welch MJ. Evaluation of copper-labeled bifunctional chelate-albumin conjugates for blood pool imaging. *Nucl Med Biol*. 1993;20:461–467.
10. Wängler B, Quandt G, Iovkova L, et al. Kit-like ¹⁸F-labeling of proteins: synthesis of 4-(di-tert-butyl[¹⁸F]fluorosilyl)benzenethiol (Si[¹⁸F]FA-SH) labeled rat serum albumin for blood pool imaging with PET. *Bioconjug Chem*. 2009;20:317–321.

11. Niu G, Lang L, Kiesewetter DO, et al. *In vivo* labeling of serum albumin for PET. *J Nucl Med*. 2014;55:1150–1156.
12. Gibson JG, Evans WA. Clinical studies of the blood volume. I. Clinical application of a method employing the azo dye “Evans Blue” and the spectrophotometer. *J Clin Invest*. 1937;16:301–316.
13. Spahr PF, Edsall JT. Amino acid composition of human and bovine serum mercaptalbumins. *J Biol Chem*. 1964;239:850–854.
14. Torabi M, Aquino SL, Harisinghani MG. Current concepts in lymph node imaging. *J Nucl Med*. 2004;45:1509–1518.
15. Yan J, Manaenko A, Chen S, et al. Role of SCH79797 in maintaining vascular integrity in rat model of subarachnoid hemorrhage. *Stroke*. 2013;44:1410–1417.
16. Lang L, Li W, Guo N, et al. Comparison study of [¹⁸F]FAI-NOTA-PRGD2, [¹⁸F]FPPRGD2, and [⁶⁸Ga]Ga-NOTA-PRGD2 for PET imaging of U87MG tumors in mice. *Bioconjug Chem*. 2011;22:2415–2422.
17. McBride WJ, D’Souza CA, Sharkey RM, et al. Improved F-18 labeling of peptides with a fluoride-aluminum-chelate complex. *Bioconjug Chem*. 2010;21:1331–1340.
18. McBride WJ, Sharkey RM, Karacay H, et al. A novel method of F-18 radiolabeling for PET. *J Nucl Med*. 2009;50:991–998.
19. Baeuerle PA, Gires O. EpCAM (CD326) finding its role in cancer. *Br J Cancer*. 2007;96:417–423.
20. Carlton JE, Hayes RL. Rapid separation of generator-produced gallium-68 from EDTA eluate. *Int J Appl Radiat Isot*. 1971;22:44–45.
21. *Guide for the Care and Use of Laboratory Animals*. Bethesda, MD: National Institutes of Health; 1985. NIH publication 85-23.
22. Sun X, Niu G, Yan Y, et al. Phage display-derived peptides for osteosarcoma imaging. *Clin Cancer Res*. 2010;16:4268–4277.
23. Lassmann M, Chiesa C, Flux G, Bardies M. EANM Dosimetry Committee guidance document: good practice of clinical dosimetry reporting. *Eur J Nucl Med Mol Imaging*. 2011;38:192–200.
24. Roivainen A, Kahkonen E, Luoto P, et al. Plasma pharmacokinetics, whole-body distribution, metabolism, and radiation dosimetry of ⁶⁸Ga bombesin antagonist BAY 86-7548 in healthy men. *J Nucl Med*. 2013;54:867–872.
25. Mitra ES, Goris ML, Iagaru AH, et al. Pilot pharmacokinetic and dosimetric studies of ¹⁸F-FPPRGD2: a PET radiopharmaceutical agent for imaging αvβ3 integrin levels. *Radiology*. 2011;260:182–191.
26. International Commission on Radiological Protection. The 2007 recommendations of the International Commission on Radiological Protection. ICRP publication 103. *Ann ICRP*. 2007;37:1–332.
27. Marrero JA, Ahn J, Rajender Reddy K. ACG clinical guideline: the diagnosis and management of focal liver lesions. *Am J Gastroenterol*. 2014;109:1328–1347, quiz 1348.
28. Wang Y, Lang L, Huang P, et al. *In vivo* albumin labeling and lymphatic imaging. *Proc Natl Acad Sci USA*. 2015;112:208–213.
29. Giger M, Baumgartner HR, Zbinden G. Toxicological effects of Evans blue and Congo red on blood platelets. *Agents Actions*. 1974;4:173–180.
30. Goins B, Phillips WT, Klipper R. Blood-pool imaging using technetium-99m-labeled liposomes. *J Nucl Med*. 1996;37:1374–1379.
31. Duran R, Ronot M, Kerbaol A, Van Beers B, Vilgrain V. Hepatic hemangiomas: factors associated with T₂ shine-through effect on diffusion-weighted MR sequences. *Eur J Radiol*. 2014;83:468–478.
32. Jang HJ, Kim TK, Lim HK, et al. Hepatic hemangioma: atypical appearances on CT, MR imaging, and sonography. *AJR*. 2003;180:135–141.
33. Caseiro-Alves F, Brito J, Araujo AE, et al. Liver haemangioma: common and uncommon findings and how to improve the differential diagnosis. *Eur Radiol*. 2007;17:1544–1554.
34. Silva AC, Evans JM, McCullough AE, Jatoti MA, Vargas HE, Hara AK. MR imaging of hypervascular liver masses: a review of current techniques. *Radiographics*. 2009;29:385–402.
35. Hussain SM, Semelka RC. Hepatic imaging: comparison of modalities. *Radiol Clin North Am*. 2005;43:929–947.
36. Ronaldson PT, Davis TP. Targeting blood-brain barrier changes during inflammatory pain: an opportunity for optimizing CNS drug delivery. *Ther Deliv*. 2011;2:1015–1041.
37. McDonald DM, Choyke PL. Imaging of angiogenesis: from microscope to clinic. *Nat Med*. 2003;9:713–725.